Soft Science

Research Article

Remarkable interfacial dielectric relaxation of physically cross-linked ice hydrogels

Yongqiang Li[1], Wenjing Zhai[1], Bo Liu[2], Chuanfu Li[1], Lin Lin[3], Zhibo Yan[1], Xiangping Jiang[4], Wenguang Liu[2], Junming Liu[1]

[1]Laboratory of Solid State Microstructures, Nanjing University, Nanjing 210093, Jiangsu, China.
[2]School of Materials Science and Engineering, Tianjin University, Tianjin 300354, China.
[3]Department of Applied Physics, College of Science, Nanjing Forestry University, Nanjing 210037, Jiangsu, China
[4]School of Materials Science, Jingdezhen Ceramic Institute, Jingdezhen 333001, Jiangxi, China.

Correspondence to: Assoc. Prof. Zhibo Yan, Laboratory of Solid State Microstructures, Nanjing University, 22 Hankou Road Goulou District, Nanjing 210093, Jiangsu, China. E-mail: zbyan@nju.edu.cn

Abstract

In the conventional scenario, it is believed that hydrogels typically consist of two-phase coexisting structures based on polymer structural networks filled with water droplets and that the polymer-water interfacial layer may not be a substantial component in determining their structure and functionality. Unfortunately, it is challenging to unveil the properties of the interfacial layer, if any, owing to the multiphase nature and structural complexity of hydrogels. In this work, the morphology and microstructures of the well-known non-covalent bonding dominant polyacrylonitrile-based hydrogels are characterized and it is confirmed that the as-prepared hydrogels do consist of polymer networks and filled water droplets. The dielectric relaxation behavior in the ice hydrogel state with different water/ice contents is investigated in detail by means of dielectric relaxation spectroscopy, in order to avoid the electrode polarization effect, which is non-negligible in liquid hydrogels, particularly in the low-frequency range. The dielectric relaxation spectroscopy data demonstrate the remarkable dielectric response contributed from the polymer-ice interfacial layer, which likely accommodates a high density of polar molecules/dipoles. The temperature-dependent dielectric relaxation behavior of the ice hydrogels with different water contents is discussed and the thermal activation energy for the interfacial polar structure may be likely extracted from the dielectric loss peak data. It is found that this energy is approximately consistent with the typical bonding energy of non-covalent bonding dominant hydrogels. This study represents a substantial step towards understanding the interfacial coupling in hydrogels, an issue that has not yet been thoroughly considered.

INTRODUCTION

Hydrogels represent a class of soft and wet materials consisting of three-dimensional (3D) cross-linked networks that can hold a high content of water. The most well-known hydrogel is jelly[1]. While the chemical and/or physical cross-linking of polymer chains maintain the structural integrity of hydrogels, many hydrophilic groups, such as $-NH_2$, $-COOH$, $-OH$, $-CONH_2$, $-CONH-$ and $-SO_3H$, can be introduced so that a large amount of water can be absorbed into these networks (53.3%-95.6% water occupation in volume)[2-5]. Due to their specific microstructure and chemical bonding nature, hydrogels possess many unique properties, including stimuli-responsiveness, shock absorption, low sliding friction, flexibility and so on[6], and thus significant potentials in environmental engineering, flexible electronics and biomaterials[7-11]. While hydrogels contain water and polymer phases, their interconnected composites consist of network-like gels. Usually the polymer phase can be categorized into two classes, i.e., polymers dominated by covalent bonding and polymers dominated by non-covalent bonding. The corresponding hydrogels are known as covalently and non-covalently bonded hydrogels, respectively. Most hydrogels are more or less mechanically weak and brittle, due to the non-homogeneous cross-linking and dominant covalent bonding[2,6].

On this basis, the need to design hydrogels with favorable properties, such as enhanced strength, toughness, processability and dynamic adaptability, is urgent[12-14]. One approach is to introduce more non-covalent bonds[15]. Polymer chains with non-covalent bonding, including hydrophobic, H bonding, ionic/electrostatic and van der Waals interactions, have been widely introduced, allowing not only for excellent mechanical properties but also sensitivity to various environmental stimuli[5,12,16-19]. Consequently, these hydrogels are considered as smart hydrogels with balanced mechanical properties, rapid responses and intelligent functionalities[11,19].

Various non-covalently bonded hydrogels have been synthesized. For example, Li *et al.*[20] designed a hybrid hydrogel network, in which the crystalline polymer [poly(vinyl alcohol)] phase maintains the structural stability and reversibility and the covalently cross-linked hydrophilic polymer [polyacrylamide (PAAm)] phase maintains the network elasticity. Polyacrylonitrile (PAN)-based hydrogels represent one class of hybrid hydrogels that have significant attention recently. Bai *et al.*[21] reported the identification of various non-covalent bonds in PAN-based hydrogels and they found that the dipole-dipole interaction contributes to their high mechanical strength with excellent fatigue resistance. A similar strategy can be extended toward multiple non-covalent bonding, such as dual physical coupling that combines the dipole-dipole pairing and H bonding into the hydrogel networks[4,22]. Nowadays, this has become a universal method for improving hydrogel performance and the non-covalent interactions are the essential ingredients to achieve high stability and reversibility[12,23].

In order to understand the underlying mechanism for these functionalities, advanced characterization has become an issue of concern. Structurally, for 3D hydrophilic polymeric networks, the filled water phase may be viewed as a composite of a free water phase, which can flow freely, and a bound water phase that is confined in the polymer-water interfacial layer. Therefore, the dynamic behavior of the bond coupling inside the interfacial layer should be comprehensively understood. Nevertheless, so far, this property seems to have been less considered than the two bulk phases themselves. One may take PAN-based hydrogels as objects for discussion. The dominant non-covalent bonding in PAN-based hydrogels includes dipole-dipole coupling and H bonding corresponding to the CN-CN dipole pairs and AAm-AAm H bonds, respectively,

as schematically shown in Figure 1[4]. The hydrophilic groups, -NH$_2$, -CONH$_2$ and -SO$_3$H, associated with the polymeric chains, may also establish their non-covalent bonding with water molecules, thus allowing for a high density of interfacial polar units, as labelled with blue arrows in the interfacial layer.

Given the proposed scenario, one needs to characterize the physicochemical properties of the interfacial layer in these hydrogels so that the structure-property relationship can be established. This issue is also important for other types of hydrogels with different interfacial couplings. In fact, advanced characterization techniques have been utilized/developed to address this issue, including direct imaging and scattering spectroscopies, such as cryo-scanning electron microscopy and transmission electron microscopy[24,25], as well as Fourier infrared spectroscopy, Raman spectroscopy and neutron scattering[26-28]. It should be mentioned here that the high density of CN-CN dipole pairs, AAm-AAm H bonds and -SO$_3$H groups in PAN-based hydrogels are electrically polar. Given that hydrogels are mainly utilized in environments of relatively slow requests, low- and medium-frequency dielectric relaxation spectroscopy (DRS) could be a favored technique for probing the dynamic behavior of these polar units in the interfacial layer.

Although DRS has been extensively utilized to characterize the electric responses of hydrogels, the interfacial layer as a topic of DRS studies has been rarely touched[29-32]. This situation is more or less due to the intrinsic difficulty in the characterization itself and the structural complexity of hydrogels. A reliable separation of dielectric response of the interfacial layer from those contributed from the two bulk phases seems to be an insurmountable obstacle even though the interfacial layer's contribution is non-negligible. Furthermore, the high fraction of liquid water phase allows the polarizable water ions to aggregate onto the electrode-hydrogel interface via rapid liquid diffusion (sufficiently fast to respond to the low-frequency signals), generating the electrode polarization (EP) effect in the low-frequency range (e.g., f < 10 Hz)[33]. Therefore, this EP effect may not be large in the relatively high f range, but its magnitude is clearly sufficient to submerge all the intrinsic dielectric signals, which also decrease with increasing f.

To overcome this barrier, the EP effect in the liquid water phase must be suppressed as much as possible. An immediate approach is to replace real wet hydrogel by ice hydrogel in which liquid water is frozen into an ice phase so that the EP effect and other flowing-induced fluctuations can be avoided, since no more inter-site diffusion can occur in the ice phase. Similarly, such inter-site diffusion occurring inside the polymer phase would be largely suppressed, if any was present. Alternatively, the local fluctuations of polar molecules and electric dipoles remain less affected by the replacement of liquid water with ice. Therefore, it has come to our attention that a DRS investigation on ice hydrogel may present a strong opportunity to extract the dielectric relaxation in the interfacial layer.

In this work, our major motivation is to utilize the DRS method to characterize the dielectric response of ice hydrogels dominated by non-covalent bonding. This motivation includes two main questions, namely, whether the dielectric relaxation of the interfacial layer is remarkable or not and whether the physicochemical properties of the interfacial layer are similar to the bulk phase or not. The PAN-based hydrogels act as our object of investigation mainly due to the fact that such hydrogels contain a relatively high density of non-covalent bonds and can be used to reveal whether the interfacial dielectric response is remarkable in addition to the polymer bulk and water phases. It is thus suggested that the interfacial layer may contribute largely to the physicochemical properties of the PAN-based hydrogels, thereby being beneficial to understanding their mechanical and environmentally sensitive performance.
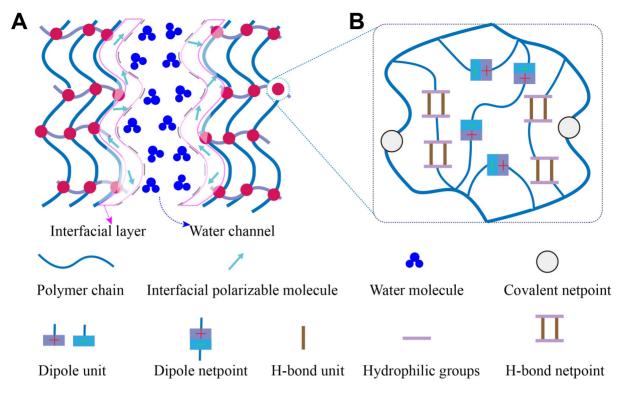
A

B

Interfacial layer   Water channel

Polymer chain   Interfacial polarizable molecule   Water molecule   Covalent netpoint

Dipole unit   Dipole netpoint   H-bond unit   Hydrophilic groups   H-bond netpoint

Figure 1. (A) Schematic of the PAN-based hydrogel network structure. (B) A typical polymer structural unit with the well-crossed PAN-based hydrogels, including the dual-physical interactions of dipole-dipole pairs and hydrogen bonds, as well as the covalent interaction. PAN: Polyacrylonitrile.

EXPERIMENTAL

Sample preparation

The PAN-based hydrogels were synthesized by the standard procedure[4]. The details of synthesis were described in earlier reports and only a brief description is given here. A schematic diagram for the chemical reaction during the synthesis is presented in Figure 2 following the information given in Ref.[4].

As an example for the synthesis process, 793 µL of dimethyl sulfoxide (DMSO) were extracted by a pipette gun to a centrifuge tub. Then, 70 mg of acrylamide (AAm) and 10 mg of 2-acrylamido-2-methyl-1-propanesulfonic acid were added into DMSO with continuous stirring until their complete co-dissolution occurred. Furthermore, 120 mg of acrylonitrile and 12.5 mg of polyethylene glycol diacrylate (PEGDA575) were added into the solution and stirred thoroughly. Finally, 6.4 mg of 2-hydroxy-4'-(2-hydroxyethoxy)-2-methylpropiophenone (IRGACURE-2959) as the photoinitiator were added into the solution and stirred in a nitrogen atmosphere until complete dissolution. Subsequently, the mixture was poured into the mold. Ultraviolet light was used to illuminate the mixture for 1 h at room temperature to polymerize it into a hydrogel. The hydrogel was taken out from the mold and soaked in sufficient ultrapure water. In order to remove the non-reacted monomers and DMSO, the water had to be refreshed every 12 h nine to ten times. The as-generated hydrogels were loaded in a beaker full of ultrapure water in a state of readiness for the subsequent processing and experiments.

Microstructural characterization

The water content in the hydrogel samples was the main priority for structural characterization. Usually, the gravimetric method is used to measure the equilibrium water content. In detail, five pieces of regularly shaped hydrogel samples were fully swollen in ultrapure water. The samples were then taken out of the
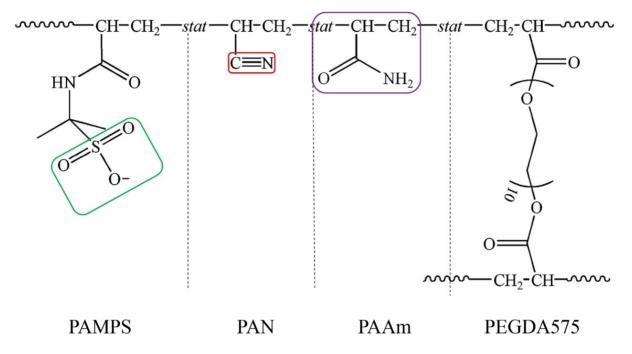
Figure 2. Schematic of the molecular structure and the basic structural units of the PAN-based hydrogel, where PAMPS, PAN and PAAm and PEGDA575 represent polyacrylamide-2-methyl-1-propanesulfonic acid, polyacrylonitrile, polyacrylamide and polyethylene glycol diacrylate, respectively. PAMPS: poly(2-acrylamide-2-methylpropanesulfonic acid); PAN: polyacrylonitrile; PAAm: polyacrylamide.

water container by removing the surface water with wet filter paper for weighing on a balance. The samples were then put in a vacuum oven at 60 °C for drying until reaching a constant weight. The equilibrium water content parameter was then calculated. In this work, we preferred to utilize the corresponding parameter f_w, the equilibrium water content in volume percentage, which seems to be more reasonable and is defined as:

$$f_w = \frac{m_w / \rho_w}{m_w / \rho_w + m_p / \rho_p}, \tag{1}$$

where m_w and m_p are the masses of the water and polymeric phases in the wet hydrogel, respectively, $\rho_w = 0.92$ g/cm³ and is the density of the ice phase and $\rho_p = 1.0684$ g/cm³ and is the density of the dried hydrogels (i.e., the polymer phase).

For characterizing the chemical bonding of the as-prepared samples, Fourier transform infrared spectroscopy (FTIR) of the hydrogels was measured using the NEXUS870 instrument manufactured by the NICOLET Company, USA. The wet hydrogels were put in the vacuum oven at 75 °C to remove the water phase in a very slow sequence. The dried hydrogels were then put into a mortar and ground into powder. The powder was dispersed in potassium bromide using a table press to press into a transparent sheet for the FTIR measurements. The wavenumber range was from 4000 to 400 cm⁻¹ and the detection accuracy was 2.0 cm⁻¹.

The microstructures at different scales were imaged by an optical camera to capture the morphology of the wet hydrogels. The morphology of the dried hydrogels as duplicates of the wet hydrogel sample was imaged by means of environmental scanning electron microscopy (ESEM) using a Quanta 200 instrument produced by the FEI Company, USA. To achieve this, the wet hydrogels were cut into regular rectangles for

photographing. For the ESEM imaging, the hydrogels were soaked in liquid nitrogen for 1 h so that the original morphology of wet hydrogels can be frozen. Subsequently, the frozen hydrogels were quickly transferred into the freeze dryer that could continually work at -50 °C for 3 to 4 day. Finally, we sprayed a thin gold film on the cross section of the final hydrogel sample to prevent charge accumulation before transferring it into the ESEM sample stage for imaging.

The crystalline-like state of the as-prepared hydrogels was analyzed by means of X-ray diffraction (XRD) using a D8 Advanced instrument manufactured by the Bruker Company, Germany. The PAN-based hydrogels in three different states were checked, including the dried, wet and ice hydrogels, in the θ-2θ mode. These samples were prepared as described below. The dried hydrogels were obtained from the wet hydrogels by a natural drying process at room temperature. The ice hydrogels were obtained by inserting the wet hydrogels into the XRD sample stage with the temperature fixed between 200 and 300 K using the liquid nitrogen cooling connection.

Furthermore, the differential scanning calorimetry (DSC) analysis of the as-prepared hydrogels was performed using the DSC-200F3 instrument manufactured by the Netzsch-Gerätebau GmbH Company, Germany. Three samples with the same water content f_w were measured by choosing heating/cooling rates of 5, 8 and 10 K/min, respectively, with the temperature T ranging from 240 to 310 K. The storage (G′) and loss moduli (G″) of the as-prepared wet hydrogels were tested using a TA Q800 dynamic mechanical analyzer (DMA) produced by the TA Instruments Corporation, USA. The sample dimensions were 15 mm in length, 6 mm in width and 0.7 mm in thickness and measured in a submersion tensile mode at 1 Hz in the warming sequence from 213 to 310 K at 2.0 K/min.

Electrical measurements

The most important experiment for this work was the DRS measurement. The wet hydrogels and pure ice plate were cut into regular shapes with 5.0 mm in length, 4.0 mm in width and 1.0 mm in thickness and a capacitor-like geometry was used for the DRS probing. For the electrode preparation, two pieces of gold foils of 5.0 mm × 4.0 mm × 0.1 mm in size were used as the top and bottom electrodes. The sample was then frozen into the ice hydrogel and pure ice states for DRS probing.

Here, it should be mentioned that the ice phase is gradually evaporated during the DRS probing due to the cryo-based temperature control if the measurement duration is long. To avoid the evaporation, the hydrogel capacitor was sealed in a plastic bag to reduce substantially the water evaporation in the cooling/warming sequences. The sample was in good contact with the temperature control stage and the cooling/warming rate remained sufficiently slow (0.5 K/min or slower) to avoid a possibly large difference in temperature between the sample core and the sample hold stage, noting that water/ice itself has relatively good thermal conductivity. A HP 4294A impedance analyzer, manufactured by the Agilent Company, USA, was used to carry out the DRS measurement in the frequency range of 40 Hz to 1.0 MHz, and the *ac* voltage signal was ~0.5 V in amplitude. It is noted that all the DRS probing was run in the warming sequence starting from 200 to 260 K. In this case, the initial water hydrogel sample sealed in the box was slowly cooled down to 200 K without any electric bias in a rate of 0.5 K/min.

RESULTS AND DISCUSSION
Microstructures and chemical bonding

Before presenting the detailed experimental results, a brief discussion of the structural units of the synthesized hydrogels, schematically shown in Figure 2, is given. The polymeric network contains three major components, namely, PAN, PAAm, and poly(2-acrylamide-2-methylpropanesulfonic acid) (PAMPS).

In addition, a cross-linker PEGDA575 is copolymerized to form the 3D network structure. This structure thus contains high-density non-covalently cross-linked units. The dipole-dipole interaction in the PAN component and the H bonding in the PAAm component constitute the dual physical-coupling mode with much lower chemical cross-linking density.

The as-prepared hydrogel sample in a plate shape is visually shown in Figure 3A with a water content f_w of ~0.78. The color, transparency and density are similar with earlier observations[4]. The morphology and network structure for this sample after the drying treatment, imaged by ESEM, are presented in Figure 3B. The polymeric network channels of different sizes are clearly imaged with a typical channel diameter of several micrometers. This observation is consistent with the proposed pattern sketched in Figure 1A for wet hydrogels, while the long tube-like channels are more or less the consequence of network deformation during the water evaporation and are not discussed further.

For the chemical bonding, we assessed the measured FTIR data of the wet hydrogel sample at room temperature, as plotted in Figure 3C. Clearly, the stretching vibration mode at 1679 cm^{-1} for C=O and the symmetric and anti-symmetric stretching vibration modes at 3353 and 3207 cm^{-1} for -NH$_2$, both located with the PAAm unit, can be identified. The stretching vibration mode at 1729 cm^{-1} for C=O was from the PEGDA575 crosslinker and the absorption peak of C≡N at 2242 cm^{-1} from the PAN unit can also be identified. Finally, the absorption peaks of O=S=O at 1186 and 1038 cm^{-1} can be assigned to the PAMPS unit[34]. Therefore, the FTIR data indicate the co-existence of the PAN, PAAm, PAMPS and crosslinker PEGDA575 units in our synthesized hydrogels, consistent with the earlier report[4], and non-covalent bonding indeed seems to be dominant.

The crystallinity of the sample in different forms, as confirmed by XRD, can be discussed based on the θ-2θ XRD spectra shown in Figure 3D. While the dry sample shows only weakly the crystalline or amorphous state of the polymer phase, indicated by the absence of any identifiable peak, the water hydrogel sample exhibits two broad peaks at 2θ ~29° and ~43°, indicating a liquid phase. It is noted here that no remarkable characteristic peak from the polymer can be seen, as expected. However, distinctly different from the two samples, the ice phase in the ice hydrogel sample is obviously in a polycrystalline state with a well-developed crystal structure, as evidenced by the existence of sharp peaks. The ice hydrogel measured at 260 K exhibited the main peaks at 2θ 22.6°, 24.3° and 26.2°, corresponding to the (100), (002) and (101) reflections of the hexagonal ice phase[35]. Meanwhile, there was a broad but weak peak at 2θ ~43°, which is likely to be from the amorphous state of the wet polymer phase. These characteristics show that the ice hydrogels include the ice and wet polymer phases, while no clear indication from the interfacial layer can be seen from the XRD data.

It should be mentioned that for the PAN-based hydrogels, earlier measurements on the microstructure revealed the possibility for three-phase coexistence, including the good crystalline, imperfect crystalline and amorphous phases, respectively, at 2θ ~16.8° corresponding to the hexagonal unit of cyano groups, at 2θ ~29.2° and ~38.6° from the amorphous water phase[36]. While the absence of any feature at 2θ ~29.2° and ~38.6° indicates no glass or amorphous water phase, the absence of any sharp feature at 2θ ~16.8° does confirm the amorphous polymer network. Therefore, it can be argued that the introduction of the PAAm unit could deteriorate the possible crystallinity of the polymeric phase seriously, noting that the strong dipole-dipole interaction would favor the polymeric crystallization[18].

While the polymer phase may not be well-crystallized, the presence of the crystallized ice phase in our samples can be further evidenced with the DSC data, even though the water phase is separated by the
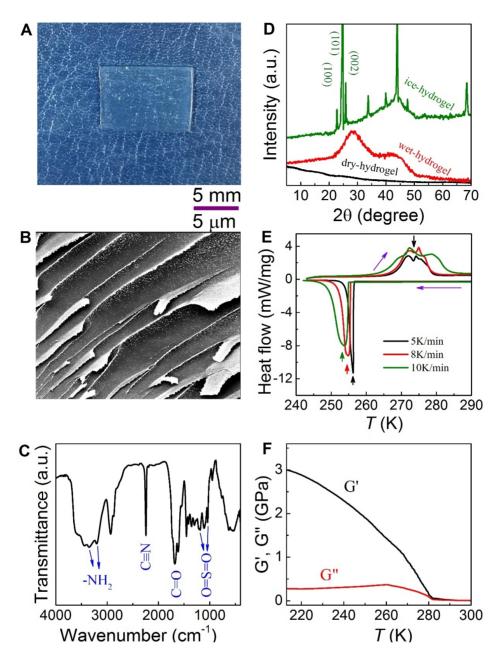
Figure 3. (A) Photograph of the as-prepared wet-hydrogel sample (f_w ~0.78). (B) ESEM image of the dry hydrogel morphology. (C) Measured FTIR spectra for the wet hydrogel sample. XRD patterns of the wet, dry and ice hydrogel samples are plotted in (D), where the well-defined reflections from the ice phase are labelled. (E) Measured DSC curves for this hydrogel sample in the cooling-warming cycle with cooling/warming rates of 5, 8 and 10 K/min, respectively. (F) Measured storage moduli (G') and loss moduli (G'') as a function of temperature T. ESEM: Environmental scanning electron microscopy; FTIR: Fourier transform infrared spectroscopy; XRD: X-ray diffraction; DSC: differential scanning calorimetry.

polymer network into small-sized droplets. The DSC data in the cooling-warming cycle are plotted in Figure 3E with three different cooling/heating rates (5, 8 and 10 K/min). While the ice-water melting sequences at the three rates show broad peaks that are located approximately at the same position, the heat-release peaks during the solidification are quite sharp with peak shifting toward the low-T side with increasing cooling rate, a typical feature for crystal solidification process from liquid water. This demonstrates that the ice phase is well crystallized in spite of the polycrystalline nature due to the polymer

network confinement.

For further identifying the crystalline state of the sample, the DMA measurement was also performed by evaluating the elastic (G′) and loss moduli (G″). It is known that G′ and G″ are the two vital quantities to characterize the elasticity and viscosity of a material[37]. The sample exhibits solid behavior if G′ ≫ G″, while it is a liquid otherwise. In the case of G′ ~ G″, the material appears to be a semi-solid, for example, the hydrogel here. The data of G′ and G″ as functions of T are plotted in Figure 3F. It is seen clearly that the two quantities coincide with each other well above 273 K, while one finds G′ ≫ G″ in the ice hydrogel state, confirming that the water phase is in a strong crystalline state. Here, it should be reminded that the loss moduli G″ at $T <$ 273 K, the ice point of water, is non-negligible even though G′ ≫ G″. This effect is essentially related to the amorphous state of the polymeric phase, contributing to the non-negligible loss moduli.

Remarkable interfacial layer contribution

After the characterization of the microstructures of the PAN-based hydrogels, clear experimental evidence is now presented to reveal that the interfacial contribution is largely detectable in terms of the dielectric relaxation. Thus, the interfacial coupling layer between the polymeric and water phases cannot be ignored when the physicochemical properties are considered.
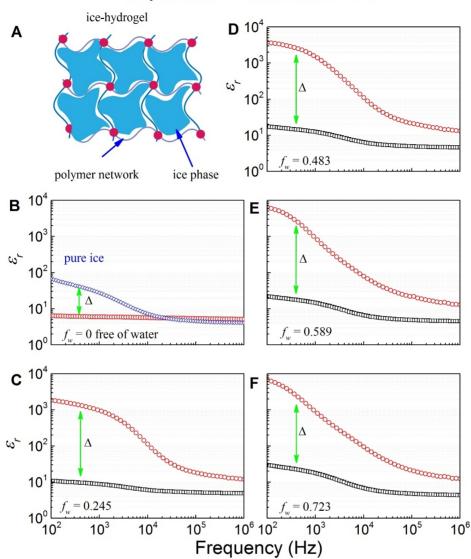
As a preparatory knowledge, we present in Figure 4A a crude schematic of the ice hydrogel sample, as inferred from the ESEM image of Figure 3B, where the ice grains and polymeric chain networks constitute a two-phase interpenetrated composite. Given a hypothesis that the sample consists of water and polymer phases only, without the interfacial layer, it is well known that the dielectric constant ε_r (real part) of such a composite structure can be described by the famous Maxwell-Garnett equation[38]:

$$\varepsilon_r = \varepsilon_p \left(1 + \frac{df_w \beta}{1 - f_w \beta} \right), \quad \beta = \frac{\varepsilon_w - \varepsilon_p}{\varepsilon_w + (d-1)\varepsilon_p}, \tag{2}$$

where ε_p and ε_w are the dielectric constants of the matrix (polymeric network) and filled particle (water/ice) phases, respectively, f_w is the water/ice content in volume fraction and d is the spatial dimension of the hydrogel structure (d = 3).

For the DRS measurement, the frequency range covered is from 100 Hz to 1.0 MHz. The dielectric constants for pure water/ice and the dried PAN-based hydrogel (i.e., dry polymer network) have been well measured, with one set of data at T ~250 K plotted in Figure 4B as an example. It saturates at ε_w ~60 in the low-f range and ε_w ~4.0 in the high-f range, with some frequency dispersion in the intermediate-f range. The dried hydrogel shows a much weaker f-dependent dielectric constant and $\varepsilon_p(f)$ ~6.0 in the whole f-range, consistent with the reported value. Given these data, one can estimate the $\varepsilon_r(f)$ data for the ice hydrogels at different f_w, as shown by the black open dots in Figure 4C-F for f_w = 0.245, 0.483, 0.589 and 0.723, where Δ indicates the difference between the calculated and measured $\varepsilon_r(f)$ data in the low-f range, noting here again that no interfacial layer is included in the model calculation.

Ideally, if the DRS signals can be simply viewed as a composite of the ice and polymer phases, the measured $\varepsilon_r(f)$ curves, the red curves, should be similar to the calculated ones from Equation (2), the Maxwell-Garnett equation, i.e., the black dot curves. Surprisingly, one finds tremendous differences between them for all the samples of different f_w. Several major features deserve highlighting. First and most importantly, for all cases,

Figure 4. Dielectric constant $\varepsilon_r(f)$ curves for all samples measured at $T \sim 250$ K with an f-range from 100 Hz to 1.0 MHz. (A) Schematic of the ice-hydrogel structural model, where the ice grains and polymeric chain networks constitute a two-phase interpenetrated composite. (B) $\varepsilon_r(f)$ curves for pure ice and dried hydrogel. (C), (D), (E) and (F) Measured $\varepsilon_r(f)$ data (open circle red dots) and evaluated $\varepsilon_r(f)$ data (open square black dots) from the Maxwell-Garnett equation [Equation (2)] for a series of samples with fw = 0.245, 0.483, 0.589 and 0.723, respectively, where indicates the difference between the calculated and measured $\varepsilon_r(f)$ data in the low-f range.

the measured $\varepsilon_r(f)$ is much larger than the calculated $\varepsilon_r(f)$. In particular, the low-f dielectric constant can be two to three orders of magnitude larger than the predicted value. Noting that the EP effect dominating in wet hydrogels is almost avoided here, this large difference must be ascribed to the contribution from the dielectric relaxation in the interfacial layer where the high density of polar molecules or dipole units may be available. Second, for the f_w dependence, it is seen that the low-f dielectric constant increases with increasing f_w until $f_w \sim 0.8$, beyond which the measured $\varepsilon_r(f)$ falls towards the value of the dried hydrogel.

The data presented in Figure 4 clearly demonstrate that the interfacial layer can be one of the major components for contributing to the dielectric relaxation of the whole hydrogel structure and likely other functionalities, according to the DRS data presented here. This issue has not been addressed previously, mainly owing to the fact that earlier DRS investigations were mainly performed on wet hydrogels instead of the ice hydrogels here. In such a case, the EP effect is somehow significant and the interfacial contribution is basically submerged. In other words, the large difference Δ may be improperly treated as the contributions of the EP effect. Here, the case is different and the PAN-based ice hydrogels are measured without significant influence from the EP effect.

Overall dielectric relaxation

The DRS measurements on a series of ice hydrogels at different f_w were performed and the data were thoroughly checked. It is not our intention in this work to discuss in detail the difference in the DRS data among these samples of different f_w. Instead, the common dielectric relaxation characters of these ice hydrogels that can reflect the interfacial layer properties will be described. As an example, the measured DRS data for sample $f_w = 0.483$ in the ice hydrogel state are shown in Figure 5A and B for the collected $\varepsilon_r(T)$ and dielectric loss $\tan\delta(T)$ at a set of frequency f, measured in the warming sequence from the low-T side to 260 K, beyond which the ice begins to melt.

At first glance, it is clear that the dielectric relaxation spectrum evidences the behavior of the bulk ice phase with strong frequency dispersion. For a given frequency f, the dielectric real part $\varepsilon_r(T)$ increases with increasing T and this increasing tendency is strong in the low-f range and becomes much weaker in the high-f range, as shown in Figure 5A. In contrast, the dielectric loss part $\tan\delta(T)$ for all frequencies demonstrates clearly the wide- and single-peaked dependence of T with the peak location at T_{max}, as shown in Figure 5B. The dielectric frequency dispersion is also evidenced by the remarkable shifting of the loss peak with increasing f.

For a clearer presentation of these relaxation features, the $\varepsilon_r(T)$ and $\tan\delta(T)$ data measured at $f = 10$ kHz are plotted in Figure 5C in the linear coordinate plane. The sharply increased $\varepsilon_r(T)$ and the broad peaked $\tan\delta(T)$ at T_{max} are more clearly presented. By extracting the values of T_{max} at a series of f, one obtains the (T_{max}, f) dataset and this is plotted in Figure 5D in the $\ln f \sim T^{-1}$ plane. One observes the linear $\ln f \sim T^{-1}$ dependence. This dependence can be more or less described by the well-known Arrhenius law[39]:

$$f = f_0 \cdot \exp(-E_a/k_B T_{max}), \tag{3}$$

where f_0 is the frequency-prefactor, k_B the Boltzmann constant and E_a the thermal activation energy for the dielectric relaxation, although its clear indication needs more discussion. The best fitting of the data gives E_a ~53.46 kJ/mol for the thermal activation energy for the dielectric relaxation.

Thermal activation energy and discussion

Given the above analysis, one is now able to discuss the influence of parameter f_w, the water content on the physicochemical properties of the ice hydrogels. The measured $\varepsilon_r(T)$ and $\tan\delta(T)$ data at four different f_w are plotted in Figure 6A and B, respectively. Beside the rapid increase with increasing T, the measured $\varepsilon_r(T)$ becomes larger at higher f_w, in particular in the T-range close to the melting point of ice. What should be considered here is the measured $\tan\delta(T)$ curves at these different f_w. Each curve exhibits remarkable and broad peak and the peak location T_{max} shifts remarkably, reflecting the strong role played by the interfacial layer. Here, two issues should be mentioned. First, the measured loss in the T-range is reasonably large and reaches $\tan\delta$ ~1.0-3.0 even at a low water content ($f_w = 0.245$), noting that the pure PAN-based polymer
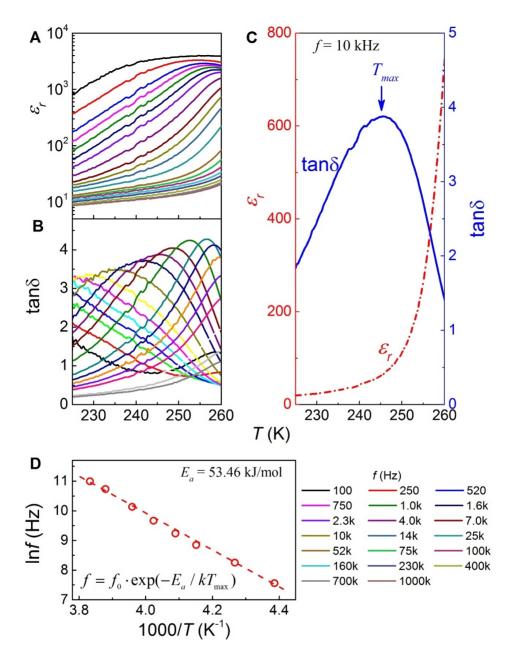
Figure 5. (A) and (B) measured dielectric real part ε_r and loss tanδ at several frequencies as a function of T for the as-prepared wet sample (f_w = 0.483) in the warming sequence from 200 K. For a clearer illustration, the measured $\varepsilon_r(T)$ and tanδ(T) data at f = 10 kHz are presented in (C). (D) Evaluated T_{max} *vs.* f relationship from which the thermal activation energy E_a is evaluated via the Arrhenius law.

phase is of very low tanδ in this T-range and the typical value is 0.02-0.03. Therefore, the loss most likely comes from the interfacial layer, noting that the bulk ice phase is well crystallized and the *d.c.* electrical conduction of the samples is very low (excluding the potential contribution from the *d.c.* conduction to the loss). Second, the strong peak shifting at different f_w also suggests the remarkable contribution from the interfacial layer. Otherwise, the loss peak would remain non-shifting although the loss intensity would increase with increasing f_w, if the loss signals would majorly come from the bulk ice phase.
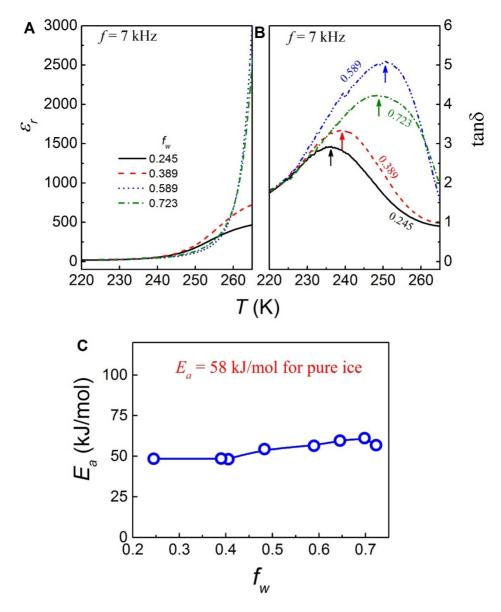
Figure 6. Measured $\varepsilon_r(T)$ and $\tan\delta(T)$ data at four different f_w are plotted in (A) and (B). (C) Evaluated E_a of the ice hydrogel samples as a function of f_w.

It has been revealed that the dielectric responses of the PAN-based hydrogels include the remarkable contribution from the interfacial layer and this is the first time this fact has been confirmed. This interfacial layer contribution would be expected to reach a maximum at $f_w \sim 0.5$, given the two-phase model scenario where the interfacial layer occupies the highest volume fraction. Indeed, it can be seen from Figure 6B that the peak is the highest for $f_w \sim 0.589$ and becomes lower again when f_w is roughly larger or smaller, e.g., the cases for $f_w = 0.389$ and 0.723 where the peak intensity and T_{max} (as indicated by the arrow) are lower than those for $f_w = 0.589$.

Finally, the thermal activation energy E_a of the ice hydrogel samples as a function of f_w should be discussed qualitatively and the evaluated values simply from the Arrhenius law are shown in Figure 6C. It is clearly seen that the activation energy is reasonably constant, i.e., 50-60 kJ/mol, roughly independent of the water

content, a reasonable outcome assuming the whole set of samples have similar interfacial coupling properties. Furthermore, the value of the pure ice phase, E_{aw}, is also ~58 kJ/mol[40,41]. The similar activation energy values between the ice hydrogels and pure ice sample suggest the similar dynamics of the electric dipoles (molecules, dipoles and other bonded units) in the interfacial layer to those polar water molecules. Considering the major non-covalent bond structure in the interfacial layer, this result is physically reasonable. Instead, one can expect much larger activation energy for these hydrogels with strong covalent bonding between the polymer phase and water.

CONCLUSION

In summary, PAN-based ice hydrogels dominated by non-covalently bonded structures have been investigated by performing a series of microstructural, thermomechanical and chemical bonding characterization. In particular, DRS of the ice hydrogel samples with different water/ice contents f_w was measured, in order to avoid the serious EP effect present in the water hydrogel state. This DRS measurement on the ice hydrogels allows for a comprehensive investigation of the polymer-water interfacial layers and their roles in determining the physicochemical properties of the hydrogels. It is revealed that this set of PAN-based hydrogels exhibits a remarkable contribution from the polymer-water interfacial layers in terms of dielectric relaxation, an effect that has been less addressed previously. The dielectric response of the hydrogel samples is largely from the interfacial layers rather than the polymer network and ice phases, at least in the low-frequency range. The present work demonstrates the substantial roles of the so far less-addressed polymer-water interfaces and sheds essential light on our understanding of the structure-property relationship in hydrogels.

DECLARATIONS

Authors' contributions
Made substantial contributions to conception: Liu J
Design of the study: Li Y, Yan Z, Liu J
Data analysis and interpretation: Li Y, Yan Z
Data acquisition: Li Y, Zhai W
Administrative, technical, and material support: Liu W, Liu B, Li C, Lin L, Jiang X, Yan Z, Liu J
Manuscript writing: Liu J, Yan Z, Li Y

Availability of data and materials
Not applicable.

Conflicts of interest
All authors declared that there are no conflicts of interest.

Ethical approval and consent to participate
Not applicable.

Consent for publication
Not applicable.

REFERENCES

1. Vázquez-González M, Willner I. Stimuli-responsive biomolecule-based hydrogels and their applications. *Angew Chem Int Ed Engl* 2020;59:15342-77. DOI PubMed

2. Gong JP. Why are double network hydrogels so tough? *Soft Matter* 2010;6:2583. DOI

3. Gong J, Katsuyama Y, Kurokawa T, Osada Y. Double-network hydrogels with extremely high mechanical strength. *Adv Mater* 2003;15:1155-8. DOI

4. Zhang Y, Li Y, Liu W. Dipole-dipole and H-bonding interactions significantly enhance the multifaceted mechanical properties of thermoresponsive shape memory hydrogels. *Adv Funct Mater* 2015;25:471-80. DOI

5. Qiu Y, Park K. Environment-sensitive hydrogels for drug delivery. *Adv Drug Delivery Rev* 2001;53:321-39. DOI PubMed

6. Chen Q, Chen H, Zhu L, Zheng J. Fundamentals of double network hydrogels. *J Mater Chem B* 2015;3:3654-76. DOI PubMed

7. Balakrishnan B, Banerjee R. Biopolymer-based hydrogels for cartilage tissue engineering. *Chem Rev* 2011;111:4453-74. DOI PubMed

8. Wegst UG, Bai H, Saiz E, Tomsia AP, Ritchie RO. Bioinspired structural materials. *Nat Mater* 2015;14:23-36. DOI PubMed

9. Deng J, Yuk H, Wu J, et al. Electrical bioadhesive interface for bioelectronics. *Nat Mater* 2021;20:229-36. DOI PubMed

10. Cao C, Hill TL, Li B, Chen G, Wang L, Gao X. Uncovering isolated resonant responses in antagonistic pure-shear dielectric elastomer actuators. *Soft Sci* 2021;1:1-19. DOI

11. Li G, Deng Z, Cai M, et al. A stretchable and adhesive ionic conductor based on polyacrylic acid and deep eutectic solvents. *npj Flex Electron* 2021;5:23. DOI

12. Wang W, Zhang Y, Liu W. Bioinspired fabrication of high strength hydrogels from non-covalent interactions. *Prog Polym Sci* 2017;71:1-25. DOI

13. Mati IK, Cockroft SL. Molecular balances for quantifying non-covalent interactions. *Chem Soc Rev* 2010;39:4195-205. DOI PubMed

14. Green JJ, Elisseeff JH. Mimicking biological functionality with polymers for biomedical applications. *Nature* 2016;540:386-94. DOI PubMed PMC

15. Rosales AM, Anseth KS. The design of reversible hydrogels to capture extracellular matrix dynamics. *Nat Rev Mater* 2016;1:15012. DOI PubMed PMC

16. Tang L, Liu W, Liu G. High-strength hydrogels with integrated functions of H-bonding and thermoresponsive surface-mediated reverse transfection and cell detachment. *Adv Mater* 2010;22:2652-6. DOI PubMed

17. Wang X, Wang J, Yang Y, Yang F, Wu D. Fabrication of multi-stimuli responsive supramolecular hydrogels based on host–guest inclusion complexation of a tadpole-shaped cyclodextrin derivative with the azobenzene dimer. *Polym Chem* 2017;8:3901-9. DOI

18. Zhang Y, Gao H, Wang H, et al. Radiopaque highly stiff and tough shape memory hydrogel microcoils for permanent embolization of arteries. *Adv Funct Mater* 2018;28:1705962. DOI

19. Koetting MC, Peters JT, Steichen SD, Peppas NA. Stimulus-responsive hydrogels: theory, modern advances, and applications. *Mater Sci Eng R Rep* 2015;93:1-49. DOI PubMed PMC

20. Li J, Suo Z, Vlassak JJ. Stiff, strong, and tough hydrogels with good chemical stability. *J Mater Chem B* 2014;2:6708-13. DOI PubMed

21. Bai T, Zhang P, Han Y, et al. Construction of an ultrahigh strength hydrogel with excellent fatigue resistance based on strong dipole-dipole interaction. *Soft Matter* 2011;7:2825. DOI

22. Lin P, Ma S, Wang X, Zhou F. Molecularly engineered dual-crosslinked hydrogel with ultrahigh mechanical strength, toughness, and good self-recovery. *Adv Mater* 2015;27:2054-9. DOI PubMed

23. Vermonden T, Censi R, Hennink WE. Hydrogels for protein delivery. *Chem Rev* 2012;112:2853-88. DOI PubMed

24. Kühlbrandt W. Biochemistry. The resolution revolution. *Science* 2014;343:1443-4. DOI PubMed

25. O'Reilly FJ, Xue L, Graziadei A, et al. In-cell architecture of an actively transcribing-translating expressome. *Science* 2020;369:554-7. DOI PubMed PMC

26. Lyon LA, Keating CD, Fox AP, et al. Raman spectroscopy. *Anal Chem* 1998;70:341R-61R. DOI PubMed

27. Paolini L, Federici S, Consoli G, et al. Fourier-transform Infrared (FT-IR) spectroscopy fingerprints subpopulations of extracellular vesicles of different sizes and cellular origin. *J Extracell Vesicles* 2020;9:1741174. DOI PubMed PMC

28. De Francesco A, Scaccia L, Lennox RB, et al. Model-free description of polymer-coated gold nanoparticle dynamics in aqueous solutions obtained by Bayesian analysis of neutron spin echo data. *Phys Rev E* 2019;99:052504. DOI PubMed

29. Li Y, Zhang C, Jia P, et al. Dielectric relaxation of interfacial polarizable molecules in chitosan ice-hydrogel materials. *J Materiomics* 2018;4:35-43. DOI

30. Zhou H, Wang M, Jin X, et al. Capacitive pressure sensors containing reliefs on solution-processable hydrogel electrodes. *ACS Appl Mater Interfaces* 2021;13:1441-51. DOI PubMed

31. Wang Y, Zeng F, Liu J, Wan Q, Guo D, Deng Y. Adaptive deformation of ionic domains in hydrogel enforcing dielectric coupling for sensitive response to mechanical stretching. *Advanced Intelligent Systems* 2020;2:2000016. DOI

32. Cai Y, Yang D, Yin R, Gao Y, Zhang H, Zhang W. An enzyme-free capacitive glucose sensor based on dual-network glucose-responsive hydrogel and coplanar electrode. *Analyst* 2021;146:213-21. DOI PubMed

33. Ishai PB, Talary MS, Caduff A, Levy E, Feldman Y. Electrode polarization in dielectric measurements: a review. *Meas Sci Technol*

    2013;24:102001. DOI

34.   Bai T, Han Y, Zhang P, Wang W, Liu W. Zinc ion-triggered two-way macro-/microscopic shape changing and memory effects in high strength hydrogels with pre-programmed unilateral patterned surfaces. *Soft Matter* 2012;8:6846. DOI

35.   Malkin TL, Murray BJ, Brukhno AV, Anwar J, Salzmann CG. Structure of ice crystallized from supercooled water. *Proc Natl Acad Sci U S A* 2012;109:1041-5. DOI PubMed PMC

36.   Gong Y, Du R, Mo G, Xing X, Lü C, Wu Z. In-situ microstructural changes of polyacrylonitrile based fibers with stretching deformation. *Polymer* 2014;55:4270-80. DOI

37.   Chaudhuri O. Viscoelastic hydrogels for 3D cell culture. *Biomater Sci* 2017;5:1480-90. DOI PubMed

38.   Markel VA. Introduction to the Maxwell Garnett approximation: tutorial. *J Opt Soc Am A Opt Image Sci Vis* 2016;33:1244-56. DOI PubMed

39.   Laidler KJ. The development of the Arrhenius equation. *J Chem Educ* 1984;61:494. DOI

40.   Popov I, Puzenko A, Khamzin A, Feldman Y. The dynamic crossover in dielectric relaxation behavior of ice I(h). *Phys Chem Chem Phys* 2015;17:1489-97. DOI PubMed

41.   Khamzin AA, Nasybullin AI, Nikitin AS. Theoretical description of dielectric relaxation of ice with low concentration impurities. *Chemical Physics* 2021;541:111040. DOI